Astron. Astrophys. 331, 392–404 (1998)

ASTRONOMY AND ASTROPHYSICS

Eigenfrequencies and optimal driving frequencies of 1D non-uniform magnetic flux tubes

H. Stenuit[1], **R. Keppens**[2], **and M. Goossens**[1]

[1] Centre for Plasma Astrophysics, K.U.Leuven, Celestijnenlaan 200B, B-3001 Heverlee, Belgium
[2] FOM-Institute for Plasma Astrophysics 'Rijnhuizen', P.O. Box 1207, 3430 BE Nieuwegein, The Netherlands

Received 30 June 1997 / Accepted 7 October 1997

Abstract. The eigenfrequencies and the optimal driving frequencies for flux tubes embedded in uniform but wave-carrying surroundings are calculated, based on matching conditions formulated in terms of the normal acoustic impedances at the flux tube boundary. The requirement of the equality of the normal acoustic impedance of the transmitted wave field with the normal acoustic impedance of the outgoing wave field selects the eigenmodes, while the equality of the ingoing and the transmitted normal acoustic impedance selects the optimal driving frequencies (Keppens 1996).

Even if the flux tube is uniform, the eigenfrequencies can be complex due to leakage of wave energy into the surroundings. The case of uniform flux tubes has been considered previously (e.g. Cally 1986), and serves as a testcase of our formalism. We extend Cally's results by taking a radial stratification of the flux tube into account. The non-uniformity of the flux tube can introduce another cause for energy loss, namely resonant absorption internal to the flux tube. When resonant absorption occurs, we must incorporate the appropriate jump conditions over the dissipative layer(s). This can be done using a simple numerical scheme as introduced by Stenuit et al. (1995).

Key words: magnetohydrodynamics (MHD) – methods: numerical – Sun: photosphere – Sun: sunspots – Sun: oscillations

1. Introduction

The linear MHD spectrum of a system consisting of a flux tube and surroundings has been investigated before, with various assumptions and simplifications. The thin tube approximation is a regularly used approximation. It enables to consider other generally excluded phenomena as gravity (Defouw 1976; Roberts & Webb 1978) or complex frequencies (Roberts & Webb 1979; Spruit 1982). Papers which admit arbitrary radius include Wentzel (1979), Edwin & Roberts (1983), and Meerson et al. (1978). Wentzel (1979) and Edwin & Roberts (1983) are concerned with real ω. While Meerson et al. (1978) allows for complex ω, but makes other restrictive assumptions. Cally (1986) allows for complex ω and calculates the leaky and non-leaky modes for uniform tubes with arbitrary radius. Other references where external propagating solutions were allowed include Čadež & Okretič (1989) for a double step profile and Rae & Roberts (1983) for slab and interface.

A leaky mode is characterized by an external solution which carries energy away from the tube. These modes are damped due to this acoustic wave leakage into the surroundings and have therefore a complex eigenfrequency. Due to this damping in time, the eigenfunctions show a growth in the external solutions with distance from the tube. Amplitudes at large distances correspond to earlier and therefore larger amplitudes within the tube.

In this paper gravity is neglected. The tube radius is arbitrary and ω is regarded as being complex, so that there can be outward travelling external waves. The method used in this paper to find eigenmodes gives us the opportunity to extend the investigation of leaky and non-leaky oscillations done by Cally (1986) to inhomogeneous flux tubes. His results for homogeneous tubes will serve thereby as a testcase for our method.

The wave fields inside and outside the flux tube can be divided into an exciting and scattered and a transmitted part. Or else in a radially incoming, radially outgoing and a transmitted field. For each of these wave fields, an impedance can be defined at the tube boundary. This (normal acoustic) impedance is the ratio of the total linear pressure perturbation and the normal velocity perturbation and is defined for a given frequency. The acoustic impedance of a medium contains information on the allowed perturbations in the medium, since it prescribes how the amplitude ratio and the phase difference between the linear pressure perturbation and the velocity field vary in space.

The boundary conditions for the total pressure perturbation and the normal velocity component may be transformed into an impedance matching criterion which we can use to select eigenfrequencies by assuming that there is no incoming, exciting or driving field. Analogously we can find the optimal driving frequencies which are defined by the condition that when the system is driven at this (complex) frequency the incoming wave

is totally absorbed by the tube. The spectrum of optimal driving frequencies is produced by inserting the assumption that there is no scattered field. These impedances and the matching criteria will be addressed in Sect. 2.

A connection between these optimal driving frequencies and the eigenfrequencies of the system was established quite recently (Goossens & Hollweg 1993; Keppens 1996). Keppens drew the attention on the difference between the real driving frequency at which maximal (not necessarily 100%) absorption occurs and the complex optimal driving frequency for which total absorption is found. Eigenfrequencies, real maximal driving frequencies and complex optimal driving frequencies are all closely related. The relation between them is more transparent since Keppens (1996) formulated it in terms of impedances.

The solving for eigenfrequencies and optimal driving frequencies will be done numerically. We therefore extend the simple numerical scheme, discussed in Stenuit et al. (1995), with the impedance matching criteria.

When we consider inhomogeneous tubes, resonant absorption may occur. The spatial variation of the equilibrium quantities induces an Alfvén and a slow continuum. When the system is driven by an impinging wave with a frequency lying in one of these continua, (a) singularity(ies) occur(s). This implies very large gradients to build up towards an infinite amplitude which can only be stopped by any sort of dissipation, which converts some of the energy into heat.

The simple scheme mentioned above treats the possible resonances by the use of the SGHR method (Sakurai et al. 1991; Goossens et al. 1995). This method derives its computational simplicity from the fact that it circumvents the numerical integration of the full dissipative equations. The method is based on jump conditions over the dissipative layer surrounding the resonance(s). These jump conditions are obtained from an asymptotic analysis of analytical solutions to simplified versions of the linear non-ideal MHD equations in this dissipative layer. The equations and the treatment of the resonances are explained in Sect. 3.

Sect. 4 gives the comparison of the results for uniform tubes with the results of Cally (1986). The results for inhomogeneous tubes are discussed in Sects. 5 and 6 respectively. Sect. 7 summarizes the main findings.

2. Impedance matching: selecting eigenmodes and optimal driving modes

Eigenfrequencies and optimal driving frequencies are selected by means of the boundary conditions of the flux tube with its infinite and wave-carrying surroundings. Across the boundary of the flux tube, both the total pressure perturbation δP and the velocity component normal to the flux tube boundary, δv_r, must be continuous (δ denotes the Lagrangian perturbation). Their ratio defines the normal acoustic impedance $Z = \delta P/\delta v_r$ (e.g. Morse & Feshbach 1953). As in Keppens (1996) we can split the external wave field into the exciting and the scattered part (part entirely due to the presence of the flux tube). Alternatively we can decompose it into radially incoming and outgoing cylindrical waves, when focussing on the geometry of the scatterer. For each of these wave fields we can define the corresponding impedance.

The continuity of δP and δv_r across the boundary can be rewritten to give the transmitted or internal normal acoustic impedance:

$$Z_{tr} = \frac{\delta P_{tr}}{\delta v_{r,tr}} = \frac{\delta P_{exc} + \delta P_{sc}}{\delta v_{r,exc} + \delta v_{r,sc}} = \frac{\delta P_{in} + \delta P_{out}}{\delta v_{r,in} + \delta v_{r,out}}. \quad (1)$$

These equalities can then be manipulated to yield:

$$\frac{\delta v_{r,sc}}{\delta v_{r,exc}} = \left(\frac{Z_{tr} - Z_{exc}}{Z_{sc} - Z_{tr}}\right), \quad (2)$$

$$\frac{\delta v_{r,out}}{\delta v_{r,in}} = \left(\frac{Z_{tr} - Z_{in}}{Z_{out} - Z_{tr}}\right). \quad (3)$$

Two important conclusions can be drawn from these equations:

- Eigenfrequencies can be found by assuming that there is no incoming wave. Thus the impedance criterion to select eigenfrequencies is $Z_{out} = Z_{tr}$ (or $Z_{sc} = Z_{tr}$).
- Optimal driving frequencies can be found by assuming that there is no outgoing wave. Thus the impedance criterion to select optimal driving frequencies is $Z_{in} = Z_{tr}$.

These conclusions give us a means to select the eigenfrequencies and the optimal driving frequencies. Therefore we define the complex impedance difference functions:

$$F(\omega) = Z_{tr} - Z_{out}, \quad (4)$$

$$G(\omega) = Z_{tr} - Z_{in}. \quad (5)$$

The eigenfrequencies are these frequencies for which F equals 0. The optimal driving frequencies correspond with the zeroes of G. Note that in general the solutions of $F = 0$ and $G = 0$ are complex.

3. Equations and solutions

We simplify the problem by Fourier analyzing in θ, z and t. All perturbed quantities are assumed proportional to

$$\exp[i(k_{\|} z + m\theta - \omega t)], \quad (6)$$

where m is an integer.

In ideal MHD, the displacements in a compressible 1D cylindrical plasma can be described by a set of two first-order differential equations for the radial component of the Lagrangian displacement, ξ_r and the perturbed total pressure P_1 (see, e.g., Appert et al. 1974):

$$D\frac{d(r\xi_r)}{dr} = C_1 r\xi_r - C_2 r P_1, \quad (7)$$

$$D\frac{dP_1}{dr} = C_3\xi_r - C_1 P_1, \quad (8)$$

where $D = \rho(c^2 + v_A^2)(\omega^2 - \omega_c^2)(\omega^2 - \omega_A^2)$. The other perturbed quantities (ρ_1, p_1,.....) can be computed once ξ_r and P_1

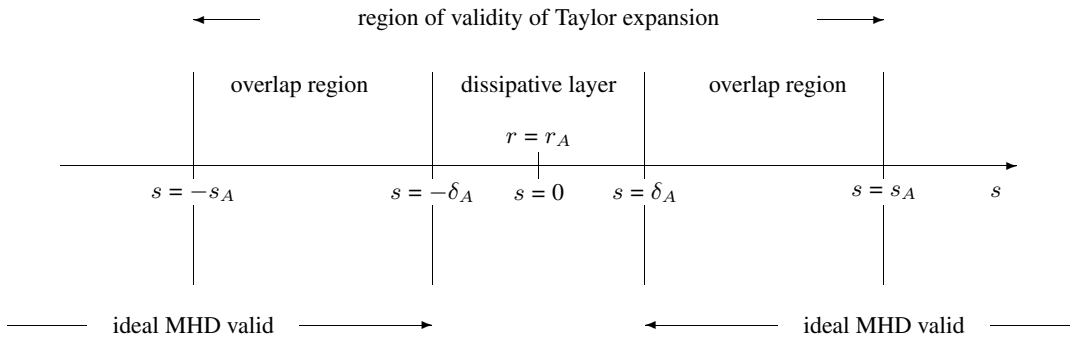

Fig. 1. Schematic overview of the notations in the treatment of the dissipative layer

are known. The sound speed and the Alfvén speed are defined as: $c^2 = (\gamma p)/\rho$ and $v_A^2 = B^2/\rho$ where the ratio of specific heats $\gamma = 5/3$, as usual. The Alfvén and cusp frequency are defined by:

$$\omega_A^2 = \frac{k^2 B^2}{\rho}, \tag{9}$$

$$\omega_c^2 = \frac{c^2 \omega_A^2}{c^2 + v_A^2}. \tag{10}$$

The coefficient functions C_1, C_2 and C_3 depend on the equilibrium quantities and on the frequency ω. When $B = (0, 0, B_z)$ (no twist in the magnetic field) then $C_1 = 0$. The coefficient C_2 can be rewritten as $C_2 = (\omega^2 - \omega_I^2)(\omega^2 - \omega_{II}^2)$ to obtain the (local) cut-off frequencies ω_I and ω_{II}:

$$\omega_I^2 = \frac{(c^2 + v_A^2)}{2} \times (\frac{m^2}{r^2} + k_\parallel^2) \times (1 - \sqrt{| 1 - \frac{4\omega_c^2}{(\frac{m^2}{r^2} + k_\parallel^2)(c^2 + v_A^2)} |}) \tag{11}$$

and

$$\omega_{II}^2 = \frac{(c^2 + v_A^2)}{2} \times (\frac{m^2}{r^2} + k_\parallel^2) \times (1 + \sqrt{| 1 - \frac{4\omega_c^2}{(\frac{m^2}{r^2} + k_\parallel^2)(c^2 + v_A^2)} |}). \tag{12}$$

To obtain the impedances at the tube boundary necessary to select eigenfrequencies and optimal driving frequencies, we have to solve the Eqs. (7)-(8) in both the internal and external region of the tube. The external region is homogeneous and non-magnetized, while the internal region is characterized by a (straight) magnetic field and (eventually) inhomogeneous equilibrium quantities.

3.1. Internal region

In a non-uniform plasma ω_A and ω_c are functions of position and they therefore determine an Alfvén and slow continuum. This gives possible singular points at r_A and r_c where:

$$\omega_A(r_A) = \omega \tag{13}$$

or

$$\omega_c(r_c) = \omega. \tag{14}$$

Jump conditions can be obtained to cross the dissipative layer and avoid solving the dissipative equations. The exact results can be found in Sakurai et al. (1991), Goossens et al. (1995) and the numerical implementation in Stenuit et al. (1995).

A new variable $s = r - r_A$ is thereby used. The treatment of the dissipative layer(s) $[-\delta_A, \delta_A]$ around the possible resonance(s) is based on an overlap region (Fig. 1) where the asymptotic dissipative MHD solutions (valid for $s \to \pm s_A$) and the simplified, ideal solutions (valid in the interval $[-s_A, s_A]$) are matched. This matching leads to jump conditions over the resonant point. Analogue for slow resonances.

For the transmitted impedance, we have to use numerical integration to obtain the internal solution. We start with a power series for ξ_r and P_1 around $r = 0$ as in Stenuit et al. (1995). The values of ξ_r and P_1 at a value r_{start} are used to start the numerical integration of the ideal MHD wave equations by use of a Runge-Kutta scheme. This Runge-Kutta integration in combination with the jump conditions yields values for P_1 and ξ_r at the boundary and therefore for the transmitted impedance. In this way we find a corresponding complex F- and G-value for each complex frequency, if the external solution is known. We subsequently iterate this procedure to locate the zeroes of these functions for a particular set of mode numbers m and $k_\parallel$.

3.2. External region

The waves in the uniform, non-magnetic region outside the flux tube are accurately described by the equations of ideal MHD. The solutions to these equations for $r \geq 1$ can be written in terms of Hankel functions as:

$$P_{1e} = \alpha_1 H_m^{(1)}(k_\perp r) + \alpha_2 H_m^{(2)}(k_\perp r) \tag{15}$$

and

$$\xi_{re} = \frac{k_\perp}{\rho_{0e}\omega^2}[\alpha_1 H_m^{(1)'}(k_\perp r) + \alpha_2 H_m^{(2)'}(k_\perp r)] \quad (16)$$

where P_{1e} and ξ_{re} denote the Eulerian perturbation of the plasma pressure and the radial component of the Lagrangian displacement in the external region. ρ_{0e} is the density outside the flux tube, and $k_\perp$ and ω are the radial wave number and frequency.

In these equations $H_m^{(1)}$ and $H_m^{(2)}$ are the Hankel functions of, respectively, the first and second order, and a prime on these symbols denote the derivative of the Hankel functions with respect to their argument.

The prescription to calculate the external horizontal wavenumber $k_\perp$ is:

$$k_\perp = \sqrt{\frac{\omega^2}{c^2} - k_\parallel^2}, \quad (17)$$

where we introduce a branch cut on the real axis as $[-k_\parallel, +k_\parallel]$ in the complex $(k_\parallel, k_\perp)$-plane and choose signs for $Re(k_\parallel)$ and $Im(k_\parallel)$ such that $Re[\frac{\omega}{c}k_\perp^*] \geq 0$ (the asterisk denotes the complex conjugate) to remove the double-valuedness of the root (see Keppens 1996).

The complex impedance difference functions then become:

$$F(\omega) = \frac{P'_{tr}}{i\xi_{r,tr}} - \frac{i(ka)}{k_\perp}\frac{H_m^{(1)}(k_\perp a)}{H_m^{(1)'}(k_\perp a)}, \quad (18)$$

$$G(\omega) = \frac{P'_{tr}}{i\xi_{r,tr}} - \frac{i(ka)}{k_\perp}\frac{H_m^{(2)}(k_\perp a)}{H_m^{(2)'}(k_\perp a)}. \quad (19)$$

4. Results: eigenfrequencies for a uniform flux tube: comparison with Cally (1986)

The characteristic uniform equilibrium quantities that we use in this paragraph will be chosen as the axial values of the non-uniform equilibrium, to make the comparison between homogeneous and inhomogeneous tubes possible. As a consequence our uniform equilibrium quantities are not exactly the same as Cally's. He also included an external magnetic field, which is neglected in our equilibrium. Therefore we exclude the possibility of fast and slow magneto-acoustic waves in the external region and consider only acoustic oscillations. The density contrast between the external and internal density equals 2.

The values and order of characteristic speeds for our uniform model are:

$$v_{Ae} = 0 = c_{Te} < c_{Ti} = 0.55 < c_i = 0.65 < c_k = 0.67 < c_e = 0.79 < v_{Ai} = 1, \quad (20)$$

when scaled to the axial Alfvén speed. The subscript 'e' or 'i' denotes the external or internal region. The tube speed is defined by $c_T = (cv_A)/(c^2 + v_A^2)$.

To compare with the characteristic speeds Cally employs, we have to multiply with a scaling factor v_{Ai}/c_e to get:

$$v_{Ae} = 0 < c_i = 0.82 < c_e = 1 < v_{Ai} = 1.26. \quad (21)$$

Our results may therefore differ from Cally's results, but the overall picture will be satisfyingly similar.

4.1. Sausage modes: $m = 0$

Fig. 2 shows numerically calculated leaky and non-leaky sausage modes. It is to be compared with Cally's dispersion diagram Fig. 1a for $m = 0$. Notice the logarithmic scale for the imaginary part in our figure.

The following modes can be distinguished (letters corresponding to those on Fig. 1 in Cally):

a) The frequency of this mode only has an imaginary part. So it can be considered as a surface perturbation diffusing into the external region. As $k_\parallel \to \infty$ it becomes one of Cally's 'cubic' modes. In the long wavelength limit, one can obtain a cubic equation in v^2, where $v = \omega/k_\parallel$ is the longitudinal phase velocity (Cally Eq. 5.14):

$$v^4(v^2 - c^2) \sim X^2(v^2 - v_A^2)(v^2 - c_e^2)(v^2 - c_T^2), \quad (22)$$

where $X = \frac{1}{d}\sqrt{\frac{v_{Ai}^2 + c_i^2}{v_{Ae}^2 + c_e^2}}$ (d is the ratio of the external to the axial density). Either one or all of the roots are real. For the photospheric values discussed above, we obtain three real roots for v^2: $v^2 = -2.237$ or $v^2 = 0.462$ or $v^2 = 0.236$ and thus two real and 1 imaginary root for v. This one is the cubic mode whose phase speed converges to the imaginary cubic root ($v \to -1.4957i$).

b) A single non-leaky slow, surface mode (S_- mode in Cally's notation), which converges to one of the two real cubic roots as $k_\parallel \to \infty$ ($v = \omega/k_\parallel \to 0.4857$). Cally also considered the thin tube approximation where R (radius of the tube) is assumed small compared with the characteristic longitudinal length scale of the waves:

$$k_\parallel R \ll 1, \quad (23)$$

$$\omega \ll 1. \quad (24)$$

When $m = 0$ and $k_\perp$ is purely imaginary, as is the case here, the phase speed v converges to c_{Ti} from below and therefore this thin tube mode corresponds to this single surface mode.

C) Two of an infinite anti-Sturmian set of body-modes (indicated by B_- modes in Cally). We use a capital letter (C) to indicate that this set includes more modes than shown. In contrast with Cally we do find a very small imaginary part for these body modes. This would mean that at least some of these body modes are also leaky. In fact, there are an infinite number of non-leaky body modes (Cally 1985), with a possible finite number at the start of the sequence being slightly leaky. We seem to have found some of these leaky modes. For both $k_\parallel \to 0$ and $k_\parallel \to \infty$ the imaginary part vanishes. In these asymptotic regions the two body modes are non-leaky. Their finite decay time is so large compared to their period that they seem like wave-solutions. As $k_\parallel \to 0$ they converge to an infinite set of thin tube modes accumulating to c_{Ti} from above.

d) A single non-leaky, surface mode (S_+ mode in Cally's notation), which converges to the second real, cubic root as $k_\parallel \to \infty$ ($v = \omega/k_\parallel \to 0.6797$).

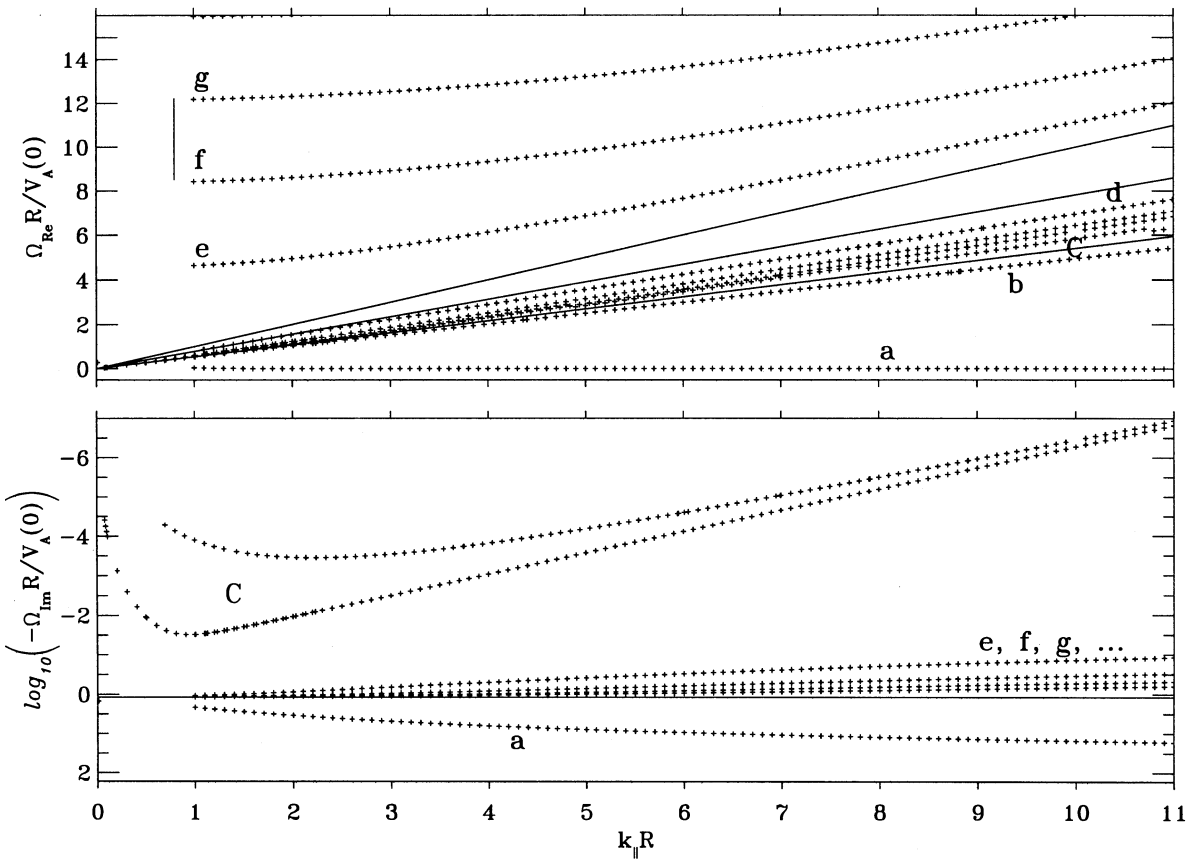

Fig. 2. Eigenspectrum for the sausage modes (m = 0) for a uniform photospheric flux tube with characteristic velocities v_{Ae} = 0, c_i = 0.65, c_e = 0.79 and v_{Ai} = 1. This spectrum can be compared with Fig. 1a in Cally (1986). Notice the logarithmic scaling for the imaginary part of the eigenfrequencies. The solid lines in the upper figure are respectively the slow, the sound and the Alfvén frequency. The different kind of modes, as discussed in the text are denoted by different letters.

e, f & g) Cally distinguishes another class of solutions, which are mostly found in the high frequency, long wavelength limit and are called 'trig' modes. Asymptotically the trig modes produce an infinite number of solutions described by Eq. 5.6 in Cally or by:

$$Im(\omega_n) = -\frac{\sqrt{v_{Ai}^2 + c_i^2}}{2} \ln(\frac{1+X}{1-X}), \tag{25}$$

$$\Delta Re(\omega_n) = \Pi\sqrt{v_{Ai}^2 + c_i^2}. \tag{26}$$

The asymptotic ($k_\parallel \rightarrow 0$) imaginary part and the spacing between the real parts can be calculated for the photospheric values discussed above:

$$Im(\omega_n) = -1.1676, \tag{27}$$

$$\Delta Re(\omega_n) = 3.748. \tag{28}$$

Therefore the trig modes are a set of infinite, nearly equally spaced eigenfrequencies which lie asymptotically along a horizontal line in the lower half ω-plane. Cally describes the eigenfrequencies to approach the real axis asymptotically as $k_\parallel \rightarrow \infty$, with $Re(\omega)$ increasing linearly with $k_\parallel$.

These three modes are respectively the first, second and third trig mode. They are leaky modes whose period and decay time are of the same order for $k_\parallel \approx 0$ and when $k_\parallel$ increases the period decreases whilst the decay time becomes long. The spacing between the real parts (as indicated by the vertical full line between f and g in Fig. 2) of subsequent trig modes and the asymptotic imaginary part (indicated with horizontal full line) is as predicted.

4.2. Kink modes: m = 1

Fig. 3 shows the dispersion diagram for the kink (m = 1) modes. The modes are completely analogous as in Fig. 2 and can be compared with Cally's Fig. 1b.

The analogy with Cally stands except for the fact that Cally only finds the cubic mode (a) for $k_\parallel R \geq 2.1$, while we do find it for the full $k_\parallel R$-range.

Apart from a few differences, the same interpretation can be made as for the sausage modes. The body kink modes found here do not have an imaginary part, in contrast with some of the body sausage modes (C) we found.

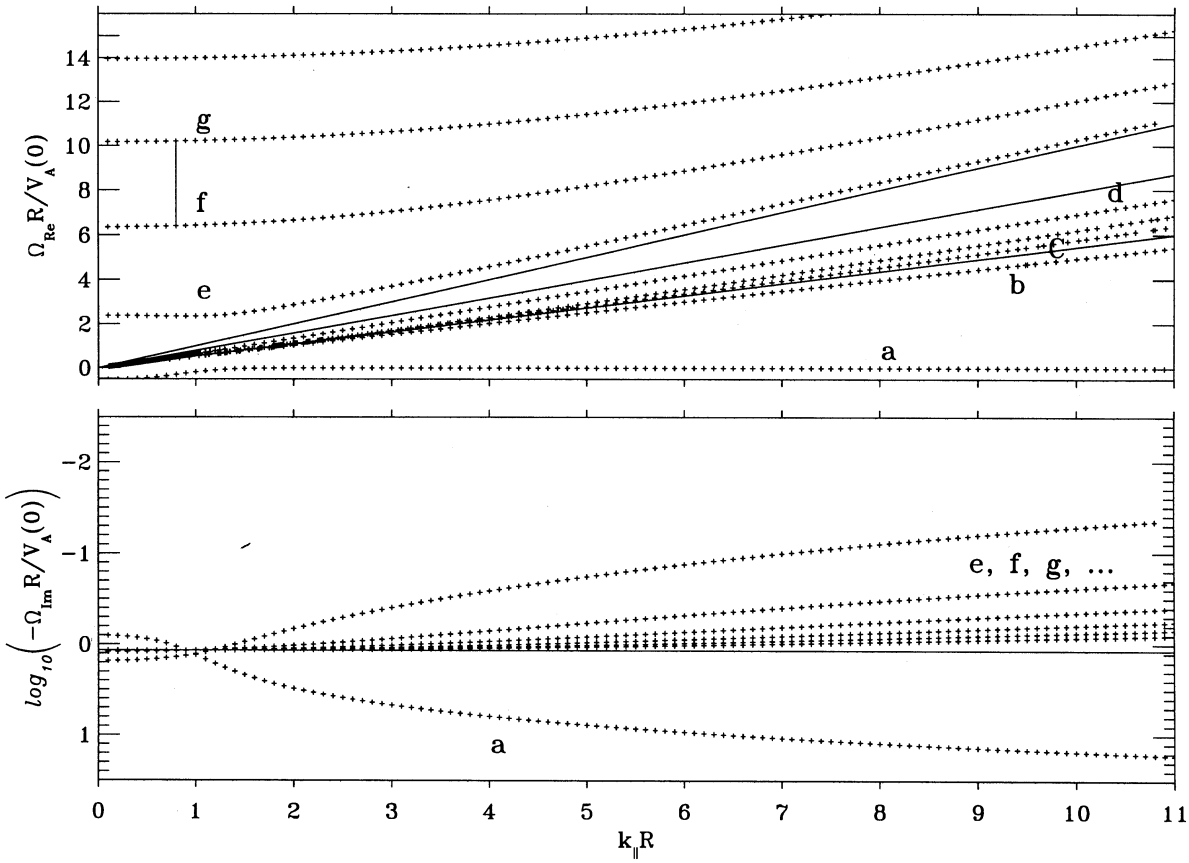

Fig. 3. Idem as in Fig. 2, but now for m = 1 (kink-modes). It can be compared with Fig. 1b in Cally (1986).

For m = 1, the phase speed in the thin tube approximation

$$v \rightarrow (\frac{\rho_i v_{Ai}^2 + \rho_e v_{Ae}^2}{\rho_i + \rho_e})^{\frac{1}{2}} = (\frac{1}{1+d})^{\frac{1}{2}} v_{Ai}, \tag{29}$$

as $k_\parallel \rightarrow 0$, which is the kink speed c_k (d is the ratio of the external and internal density). For the photospheric values used above:

$$v \rightarrow 0.57735. \tag{30}$$

5. Results: eigenfrequencies for a non-uniform flux tube

We use a generalized Lou-type (1990) equilibrium, as in Goossens and Poedts (1992) and Keppens (1996). This ideal, axisymmetric 1D MHD equilibrium is characterized by 2 parameters λ and d. The sharpness of the transition between the magnetized and the unmagnetized external region is controlled by λ. And d measures the density ratio between the external and the axial density. In the results discussed here, the choice of parameters is:

- λ = 5: a rather smooth transition from internal non-homogeneous magnetized region to the external non-magnetic surroundings
- d = 2: the external density is twice the axial density value.

If we scale the equilibrium quantities to the cylinder radius R, the total axial field $B_0(0)$ and the axial density $\rho_0(0)$, the analytical distribution of the pressure is (the subscript '0' denotes equilibrium variables):

$$p_0(r) = \frac{p_{0e}}{3}\{1 + \exp[-\lambda(r-1)^2]\}\times \\ \{1 + \tfrac{1}{2}\exp[-\lambda(r-1)^2]\}, \tag{31}$$

where p_{0e} is the dimensionless constant photospheric plasma pressure outside the flux tube.

The density profile is given by:

$$\rho_0(r) = \frac{1 + A\exp[-\lambda(r-1)^2]}{1 + Ae^{-\lambda}}, \tag{32}$$

where

$$A = \frac{1-d}{de^{-\lambda} - 1}. \tag{33}$$

The magnetic field $B_{0z}(r)$ (there is no twist in the magnetic field) is then determined from the static equilibrium condition, and varies smoothly from its axial value $B_{0z}(0)$ = 1 to zero at the flux tube radius.

Figs. 4 and 5 show the profiles of ω_A, ω_c, ω_I and ω_{II} for both m = 0 (Fig. 4) and m = 1 (Fig. 5)

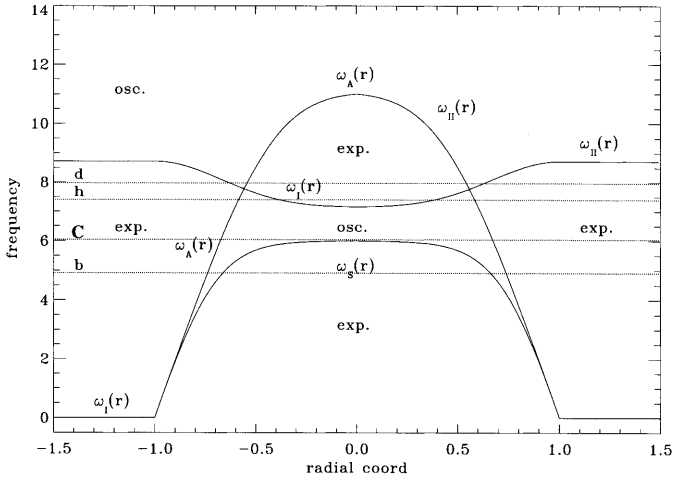

Fig. 4. Profile of Alfvén and slow frequency and of the cut-off frequencies for m = 0 and $k_\| R$ = 11 and for a non-uniform photospheric flux tube with equilibrium parameters λ = 5 and d = 2. The regions where to expect oscillatory and exponential behaviour are indicated by 'osc.' and 'exp.'. The horizontal lines (b, C, d, and h) indicate modes found at these frequencies. Their letters correspond with those in Fig. 6 and in the text.

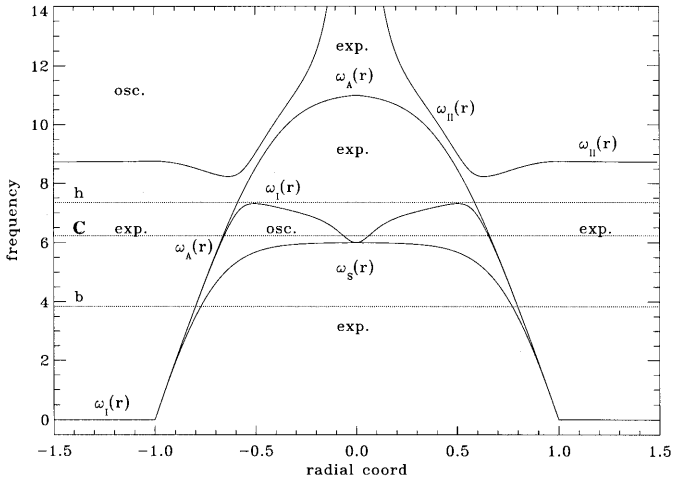

Fig. 5. Idem as Fig.4, but now for m = 1. The horizontal lines indicate modes found at these frequencies (b, C, h). The letters correspond with those found in Fig. 9 and in the text.

Depending on the ordering of the eigenfrequency with respect to ω_{II}, ω_A, ω_I and ω_c, we can determine where (in radial position) to expect oscillatory or exponential behaviour in the eigenfunctions, as indicated (by osc. and exp.) on Figs. 4 and 5. These predictions are valid for real eigenfrequencies, but even for complex frequencies, these figures still might give an idea about the kind of eigenfunctions to expect.

5.1. Sausage modes: m = 0

Fig. 6 gives the complete sausage spectrum for a non-uniform flux-tube.

For the trig modes, the picture found for the uniform flux tube remains. An infinite Sturmian set of leaky, fast, equally spaced (in real part) modes with an asymptotically constant imaginary part. When compared with the uniform tube, the real part of the frequency is decreased somewhat and the spacing between the modes is smaller. The imaginary part has a larger absolute value in the non-uniform case. The trig modes show a mainly oscillatory behaviour (as expected when looking at Fig. 4). The external solution increases with distance from the tube due to the leaky character of these modes. The first of these trig modes enters the Alfvén continuum for $k_\| R \geq 8.7$. Since there is no Alfvén resonance for m = 0, this singularity has no consequences for the eigenvalue and the eigenfunction.

The cubic mode (a) is also (partly) found. The diffusion of this perturbation happens even faster than in the uniform case due to a slightly larger (in absolute value) imaginary part of the eigenfrequency.

We followed the fast surface mode (d) in the transition from uniform to non-uniform tubes. This transition was made by changing the radial percentage of non-uniformity from 0% (entirely homogeneous internal region and discontinuity at the boundary) to 100% (inhomogeneous internal region). The eigenfunctions for the inhomogeneous tube mode are shown on Fig. 7.

When the degree of non-uniformity is increased from 0% to 100%, the typical surface perturbation at the boundary-discontinuity in the uniform case is transformed continuously into a perturbation with a peak in amplitude at the Alfvén resonant surface. This resonance moves inwards as the percentage of non-uniformity increases. For m = 0, the Alfvén resonance does not lead to jumps in the eigenfunctions however.

Fig. 4 (horizontal line indicated by d) shows that in addition to the Alfvén resonance at the eigenfrequency ω = 7.9736 ($k_\| R$ = 11), there is a dip in the ω_{II}-profile so that oscillating behaviour may be expected in this radial region. This oscillating behaviour probably provides for a continuous derivative at the peak of amplitude of the perturbation.

Due to this continuous derivative and the radial inwards shift of the perturbation, this mode looses the typical surface-like behaviour and might be characterized as a body-mode. Due to the non-uniformity and the abscence of a discontinuity the clear distinction between surface and body has faded, making the characterization of the modes more difficult.

This mode has a purely real frequency, and is thus a non-leaky mode. The external solution is therefore an exponential decreasing one.

The set of body-modes (C) is recovered in this inhomogeneous case. They are lying in the Alfvén continuum, but not in the slow continuum. But since m = 0, there are no jumps in the eigenfunction due to the Alfvén resonance. Fig. 4 shows that the behaviour of the eigenfunctions is expected to be similar for these eigenfrequencies as in the uniform case, except that the external region of exponential behaviour now reaches up to the resonant point. Once again the Alfvén resonant point in the inhomogeneous tube takes over the role of the boundary in the homogeneous tube. We could still describe this set

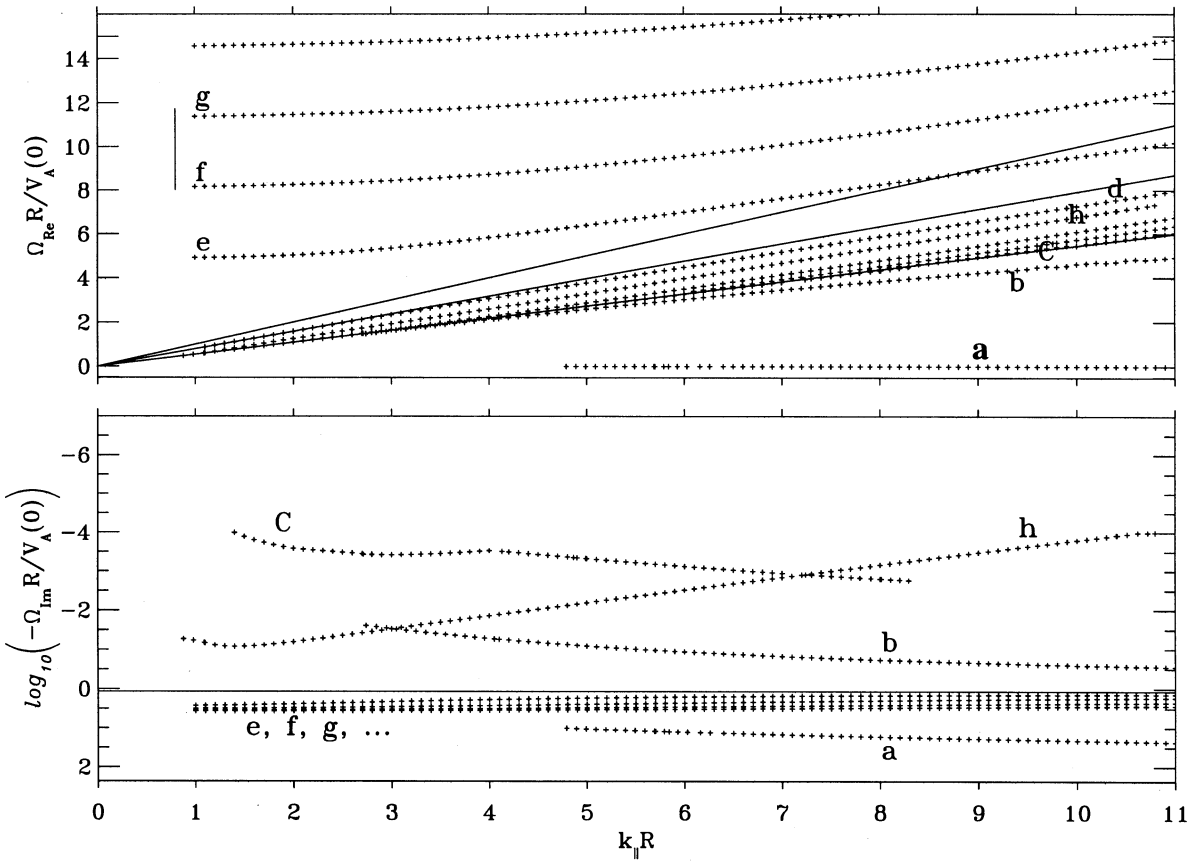

Fig. 6. Eigenspectrum for the sausage modes (m = 0) for a non-uniform photospheric flux tube. The equilibrium is characterized by a smooth transition (λ = 5) from the inhomogeneous and magnetized internal region to the uniform, unmagnetized, external region. The density contrast between the external and axial density is 2 (d). Different letters stand for different kinds of modes as discussed in the text.

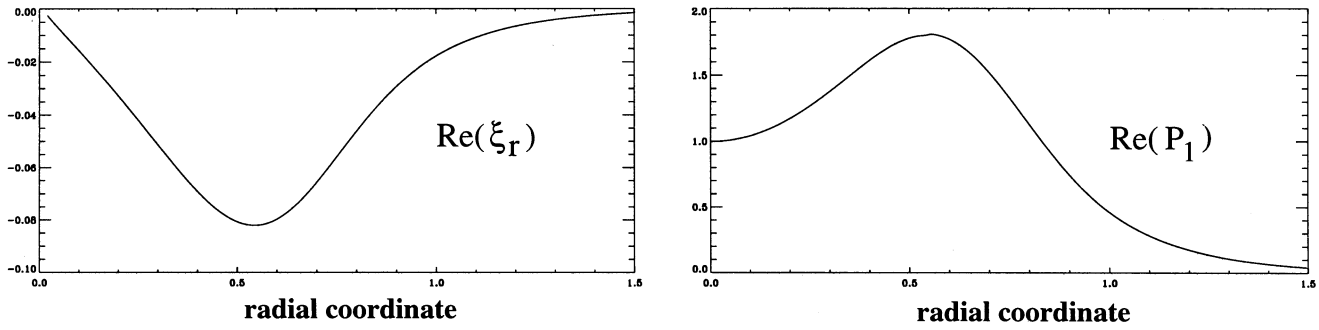

Fig. 7. The real part of the radial displacement and of the pressure perturbation (imaginary part is zero) as a function of the radial coordinate for the eigenmode ω = (7.9736, 0) ($k_\parallel R$ = 11, m = 0). This mode corresponds to a fast, surface mode in the case of a uniform tube. Due to the inhomogeneity the perturbation is shifted towards the Alfvén resonance and is rounded and looses therefore its typical surface-like behaviour. This eigenmode lies in the Alfvén continuum, but not in the slow continuum.

of modes as body-modes, although the oscillating behaviour is now restricted to a smaller region.

The set of these slow modes is still anti-Sturmian, now accumulating towards the maximum of the slow continuum. They are generally non-leaky.

There is (at least) one mode (indicated by 'h'), which has no clear explanation. Our suspicion is that it is part of this infinite set of modes (C). This would mean that, as in the case of a uniform tube, this set would start with a finite number of leaky modes. Due to the leaky character, the eigenfunctions look different than for the other (non-leaky) modes in the set. Therefore the connection is not easily made. But when looking at the case where m = 1, where all the modes of this set are leaky due to the Alfvén resonance, the corresponding 'h'-mode is recognised as the first mode of this anti-Sturmian set. The correspondence of these two 'h'-modes for different m-values is assured by making a continuous transition from one m-value to the other.

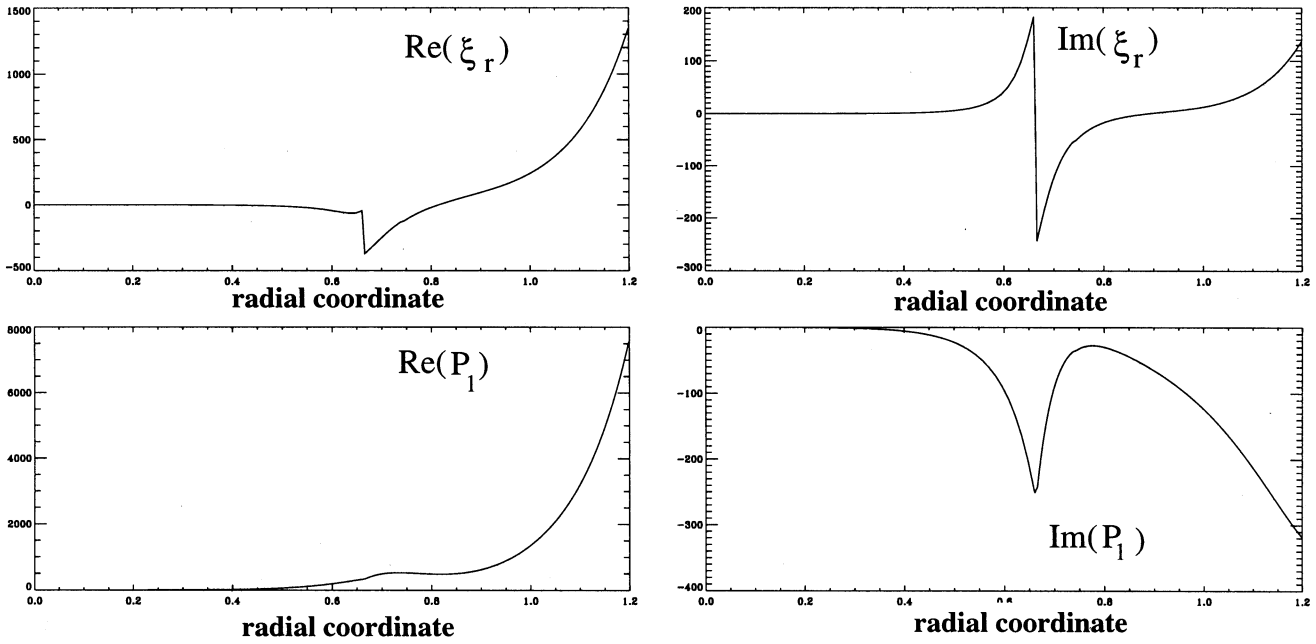

Fig. 8. The real and imaginary part of the radial displacement and of the pressure perturbation as a function of the radial coordinate for the eigenmode $\omega = (4.9196, -0.2832)$ ($k_\parallel R = 11$, $m = 0$). This eigenmode lies in both the Alfvén and slow continuum. And shows jumps over the slow resonance at $r_c = 0.66$. The Alfvén resonance is at $r_A = 0.74$, but does not provide for jumps ($m = 0$). Oscillatory behaviour is expected in between the two resonances and exponential behaviour elsewhere. In the external region the solution is increasing exponentially due to the leaky character of this mode.

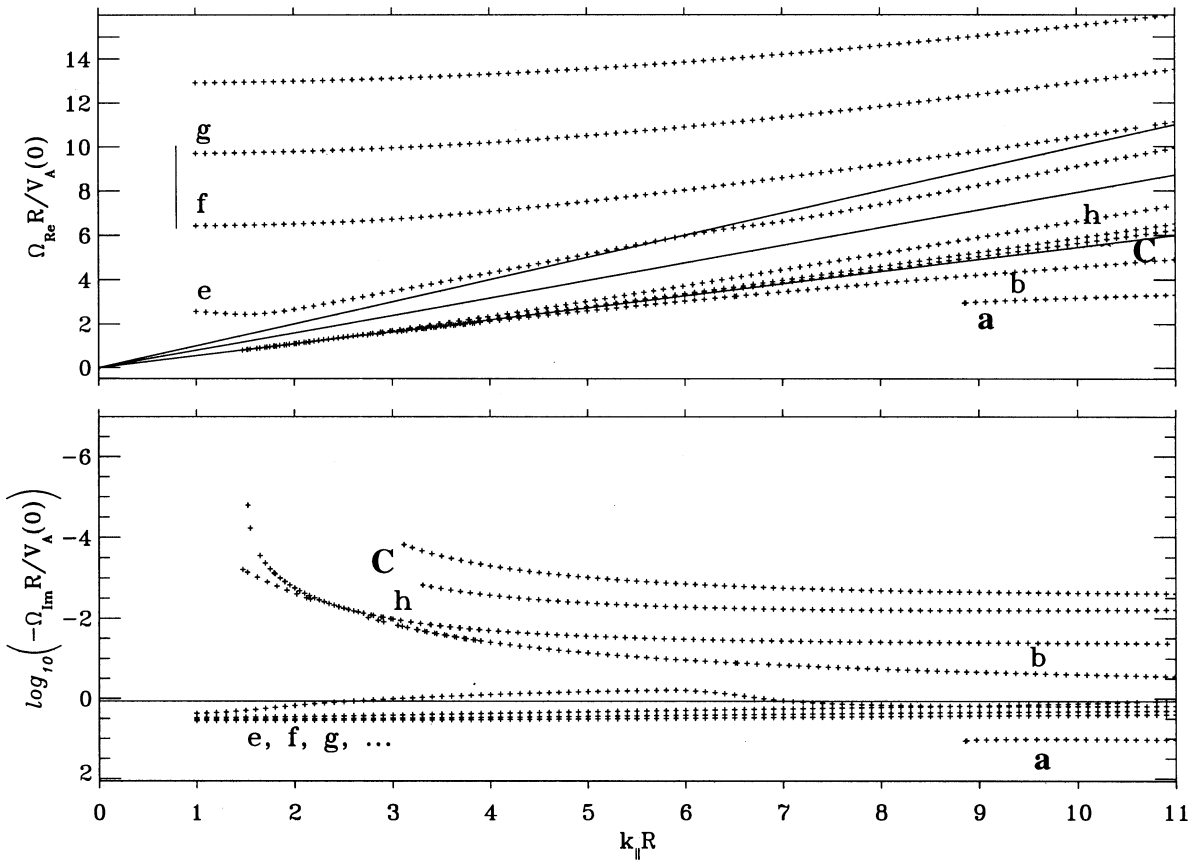

Fig. 9. Idem as in Fig. 6, but now the spectrum of the kink-modes ($m = 1$).

Also the slow surface mode (b) from the uniform case has a corresponding mode in inhomogeneous tubes. This mode now lies in both the Alfvén and slow continuum. In contrast with the uniform case, the eigenfrequency has an imaginary part, comparable in absolute value with the real part. This imaginary part is due to the slow resonance (no jumps due to Alfvén resonance when $m = 0$) and leaking. This imaginary part makes the predictions based on Fig. 4 less certain since only the real part of the frequencies is considered there. Nevertheless we suspect from Fig. 4 a similar story as for the fast surface mode. We expect (mainly) exponential behaviour in the region external to the Alfvén resonance, (mainly) oscillatory in between the two resonances and again (mainly) evanescence internal to the slow resonance. These features are recognized in the eigenfunctions in Fig. 8. Again the exponentially increasing solution external to the tube is due to leaky propagation of the perturbations in the external medium.

5.2. Kink modes: $m = 1$

We move over to the kink-modes ($m = 1$). The spectrum can be seen in Fig. 9. The main difference is that now there are jumps over the Alfvén resonance that may play a role. All eigenfrequencies in the Alfvén continuum now have an imaginary part and therefore give a complex $k_\perp$ with both a real and an imaginary part. Thus the external solution is propagating and exponentially increasing with distance from the tube.

For the so-called trig modes (e, f, g) with frequencies with real part above both continua, we expect and find a similar picture as for the sausage trig modes, as they are not affected by the Alfvén resonance. Only the first trig mode 'e' moves into the Alfvén continuum from $k_\parallel R \approx 5.8$. As seen on Fig. 5 the internal region where evanescent behaviour is expected becomes larger as the real part of the frequency decreases. Nevertheless the character of the mode shows hardly any difference for the first trig modes from that of the others. Except for the fact that the eigenfunctions are influenced by an Alfvén resonance.

The mode (b) that lies in both the Alfvén and slow continuum and that corresponds to the slow surface mode in the uniform case is also recovered. Looking at Fig. 5 and comparing the horizontal line indicated by 'b' with the one in Fig. 4, we expect similar eigenfunctions as in the $m = 0$ case (Fig. 8), except that around $r = 0.72$ they now show a small jump (in the imaginary part of the radial displacement) due to the Alfvén resonance.

The set of infinite modes (C) in the Alfvén continuum converging towards the top of the slow continuum is still present, as it was for $m = 0$. But these eigenfrequencies now have an imaginary part, probably due to the effect of the Alfvén resonance. When looking at Fig. 4 and 5 (horizontal line indicated by 'c'), once more we expect little difference in the internal solutions with the case where $m = 0$. Except that the eigenfunctions are now highly influenced by the jumps due to the Alfvén resonance. The external solution is now exponentially increasing with distance from the tube.

The mode indicated by 'h' is probably the first mode of this infinite anti-Sturmian set. It shows one node in the solution for ξ_r and none in the solution for P_1 (Fig. 10). As expected from Fig. 5, the eigenfunctions have a mainly exponential behaviour, supplemented with jumps due to the Alfvén resonance.

The 'd'-mode, corresponding to the fast surface mode in the uniform tube case, is not refound in the case where $m = 1$.

6. Results: optimal driving frequencies

6.1. Sausage modes: $m = 0$

The complex optimal driving frequencies are deduced as the nodes of the function G (26). Comparing equations (25) and (26) yields only a difference in the kind of Hankel functions. For finding the eigenvalues we use the Hankel functions of the first kind (outgoing), and to find optimal driving frequencies we use Hankel functions of the second kind (incoming).

The Hankel functions of the 1st and 2nd kind have a connecting equation which tells us exactly where to look for optimal driving frequencies in the case of no resonance. Since:

$$H_m^1(z^*) = (H_m^2(z))^* \tag{34}$$

(where the asterisk denotes the complex conjugate) and since the complex conjugated solutions for a frequency equal the solutions for the complex conjugated frequency, it follows that the optimal driving frequencies are the complex conjugates of the eigenfrequencies in the case where $m = 0$ and as long as they are lying above the slow continuum (there is no Alfvén resonance when $m = 0$).

These optimal driving frequencies with a positive imaginary part give, as noted by Keppens (1996) only an apparent 100% absorption. At these frequencies, one drives with an amplitude that grows in time, so that the lag of the amplitude growth of the outgoing wave with respect to the incoming perturbance appears as a total absorption.

The only sausage eigenmode for which it is interesting to look for its corresponding optimal driving frequency, when $m = 0$, is the d-mode (mode corresponding with the slow surface mode in the uniform case). Indeed this mode is lying in the slow continuum and the simple way to deduce the corresponding optimal driver is no longer valid. We do indeed find for the corresponding optimal driver of this mode a negative imaginary part, which implies no apparent 100% absorption, but a physically interesting optimal driving frequency, based only on the slow continuum.

6.2. Kink modes: $m = 1$

In the search for the kink modes, we used the arguments put forward in Goossens & Hollweg (1993) and Keppens (1996). The general results there are that

1) total absorption at a real frequency only takes place when the equilibrium is fine-tuned, since total absorption requires the simultaneous equality of resistances (real parts of impedances) and reactances (imaginary parts)

2) under most conditions, the difference $Z_{sc} - Z_{in}$ is small, which is why leaky modes, optimal driving frequencies, and

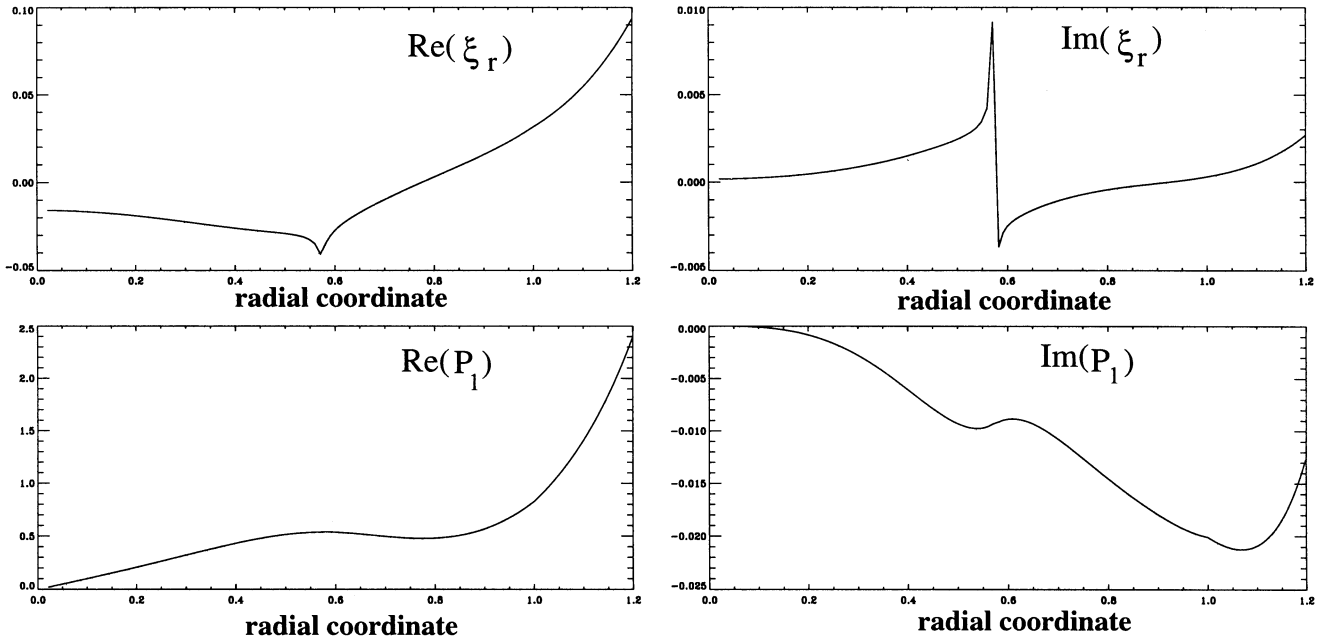

Fig. 10. The radial displacement and the pressure perturbation as a function of the radial coordinate for the eigenmode $\omega = (7.5710, -0.4653 \times 10^{-1})$ ($k_{\|}R = 11$, $m = 1$). This mode is the one indicated by 'h' in Fig. 9. It is the first mode of an infinite, anti-Sturmian set of modes accumulating towards the top of the slow continuum. These eigenfunctions show clear jumps at $r = 0.57$ due to the Alfvén resonance.

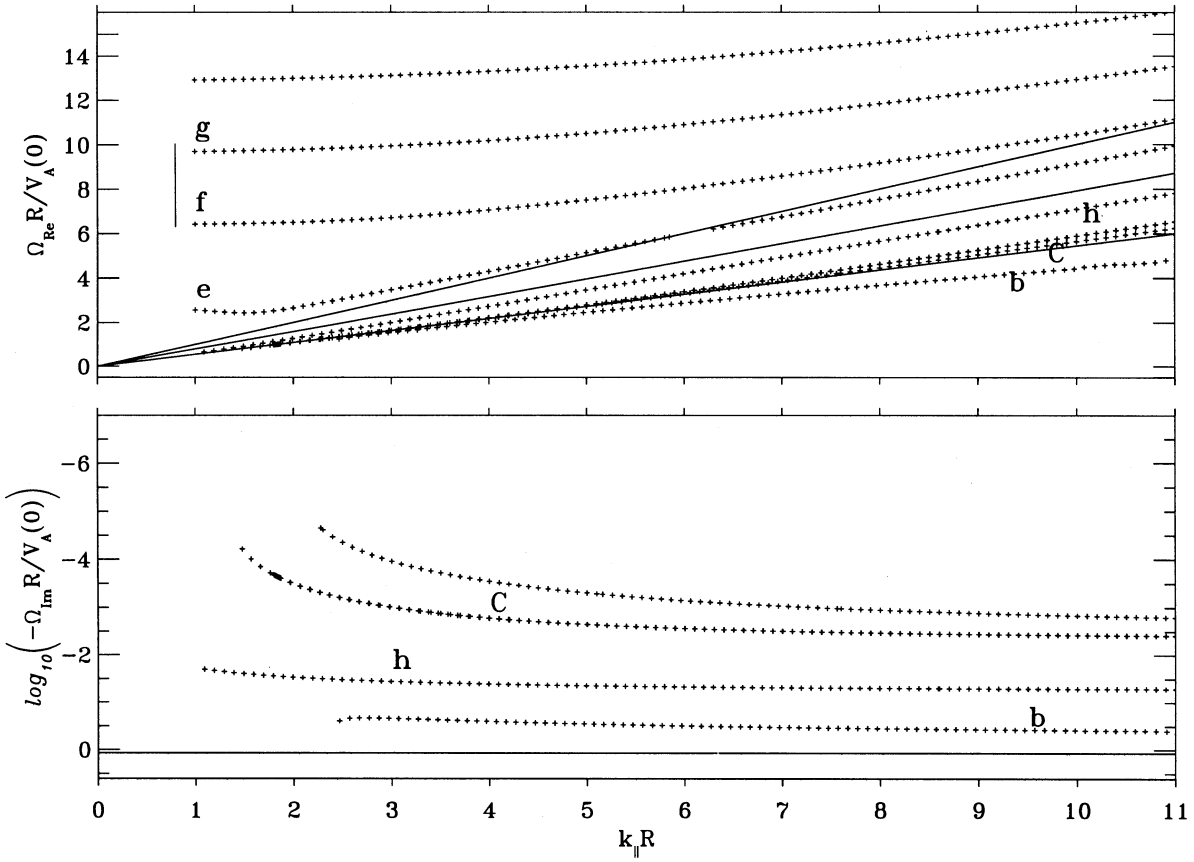

Fig. 11. Optimal driving spectrum for $m = 1$ for a non-uniform photospheric flux tube with the same equilibrium parameters as before. Compare with Fig. 9 to notice that the real parts of the different modes are quasi identical.

the real driving frequencies corresponding to maxima in the absorption coefficients are all closely connected.

This means that, when looking for optimal driving frequencies in the m = 1-case, we can use the eigenfrequencies as input-frequencies and expect to find the optimal driving frequencies in the neighbourhood of these eigenfrequencies. The complete spectrum of optimal driving frequencies for m = 1 is shown in Fig. 11.

The trig modes can be treated in the same way as most of the sausage modes by taking the complex conjugate of the eigenfrequencies. Hence the trig optimal driving frequencies are again only apparent optimal drivers and are physically uninteresting. Even the first trig mode that does enter the Alfvén continuum has a positive imaginary part and is therefore an apparent optimal driver.

All the other modes are influenced by the slow or/and the Alfvén continuum and for all of the other modes, we do find a corresponding optimal driving frequency, with a real part very close to the corresponding eigenfrequency. Comparison of the upper parts of Fig. 9 and 11 hardly shows any difference in the real parts of these modes. In general we could say that the damping is larger for the optimal driving frequencies, especially for small $k_{\|}R$.

When we consider a driven problem, the purely real driving frequency can never equal one of these optimal driving frequencies, since they all have a non-zero imaginary part. This means that when we drive with a frequency, we can never expect total absorption of the modes. We can only look for driving frequencies at which maximal (not 100 %) absorption occurs.

7. Conclusions

We developed a new method in the framework of the full understanding of both Alfvén and slow resonant absorption. This method is a derivative of the numerical scheme, used before to calculate resonant absorption in non-uniform flux-tubes. This scheme included the SG&H prescription to treat both slow and Alfvén resonant absorption and used numerical integration to deal with the non-uniform internal region.

We extended this method to derive the spectrum of eigenmodes and the spectrum of optimal driving frequencies for 1D non-uniform flux-tubes. We used the equality of the scattered and the transmitted normal acoustic impedances to select eigenfrequencies and the equality of incoming and transmitted acoustic impedances to find the optimal driving frequencies. These impedance criteria prove extremely useful and are rather transparant to work with. This method allows for general complex frequencies and therefore for the possibility for acoustic leakage into the surroundings.

We recovered the results for uniform flux-tubes found by Cally (1986) for both sausage and kink modes. The overall picture is satisfyingly similar, although the equilibria are not identical. But some small differences were noticed. We found a few of the slightly leaky modes that seems to start the infinite, anti-Sturmian set of non-leaky body modes that Cally has found. And when m = 1 we completed the cubic surface perturbation (a) for small $k_{\|}R$, while Cally found this for $k_{\|}R \geq 2.1$ only.

The recovery of these results for uniform tubes allowed us to extend to inhomogeneous tubes. We fixed the equilibrium-parameters and kept them the same throughout all the calculations. In general there seems to be a one-to-one correspondence with the modes for uniform tubes. Only the fast surface mode found for uniform tubes is not recovered for inhomogeneous tubes when m = 1. When m = 1 all of the modes become leaky in a non-uniform tube due to the resonances.

Due to the non-uniformity and the associated absence of discontinuity, the clear distinction between surface and body-modes has faded, as seen for the fast surface mode that we found in the uniform case and followed in the transition to non-uniform tubes. The role of the boundary in the uniform tubes is reduced to merely a place where some of the derivatives of equilibrium variables are not continuous and is partly taken over by the Alfvén resonant point. A surface perturbation in a uniform tube is now shifted towards the resonance. The Alfvén resonance also marks the regions where oscillating or exponential behaviour is expected, as did the boundary of a uniform tube.

We defined the optimal driving frequencies as those frequencies for which 100% absorption occurs and looked for them starting from the eigenfrequencies. There are two kinds of optimal driving frequencies. The first category are the physically uninteresting, apparent optimal drivers, which have a positive imaginary part and thus an exponentially growing amplitude. Most of the sausage optimal drivers and some of the kink optimal driving frequencies (the so-called trig modes) fall into this category. They are found as the complex conjugates of the eigenfrequencies.

In addition to these, we also find a category of physically interesting optimal driving frequencies. We found only one genuine optimal driving frequency for the m = 0-case. When m = 1, each eigenfrequency, lying in the Alfvén continuum has a corresponding genuine optimal driving frequency.

Since the transmitted normal acoustic impedance appears in both impedance criteria, eigenfrequencies and optimal driving frequencies are ultimately connected. By that the genuine optimal driving frequencies can be found by using the eigenfrequencies as a first approximation. Thus we could reevaluate the results obtained by Goossens & Hollweg (1993) and Keppens (1996), who realized this connection between eigenmodes, optimal driving frequencies and maxima in the absorption coefficients for real driving frequencies. For real driving frequencies total absorption can not be expected for the cases considered here, since all optimal driving frequencies found have a non-zero imaginary part.

Finally, we call for a similar investigation of the close connection between the slow continuum, the complex leaky modes, the optimal driving frequencies, etc., in twisted flux tube equilibria. The presence of the twist in the equilibrium may be important when studying their absorption and scattering properties. This will be addressed in a forthcoming paper.

Acknowledgements. The authors would like to thank the referee V. Nakariakov, T. Bogdan, P. Cally and V. Čadež for stimulating suggestions and interesting remarks.

References

Appert, K., Gruber, R., and Vaclavik, J.: 1974, Phys. Fluids 17, 1471.
Čadež, V. M. and Okretič, V. K.: 1989, J. Plasma Phys. 41, 23.
Cally, P. S.: 1985, Aust. J. Phys. 38, 825.
Cally, P. S.: 1986, Solar Phys. 103, 277.
Chen, L. and Hasegawa, A.: 1974, Phys. Fluids 1, 205.
Davila, J. M.: 1987, Astrophys. J. 317, 514.
Defouw, R. J.: 1976, Astrophys. J. 209, 266.
Edwin, P. M. and Roberts, B.: 1983, Solar Physics 88; 179.
Goedbloed, H.: 1984, Physica 12D, 107.
Goossens, M.: 1991, in E. R. Priest and A. W. Hood (eds.), 'MHD Waves and Wave Heating in Non-Uniform Plasmas' Advances in Solar System Magnetohydrodynamics, Cambridge University Press, Cambridge, p. 135.
Goossens, M., Hollweg, J. V.: 1993, Solar Phys. 145, 19.
Goossens, M., Ruderman, M. S. and Hollweg, J. V.: 1995a, Solar Physics 157, 75.
Hain, K., Lüst, R.: 1958, Z. Naturforsch. 13a, 936.
Hasegawa, A. and Chen, L.: 1976, Phys. Fluids 19, 1924.
Hollweg, J. V.: 1990, Computer Phys. Rep. 12, 205.
Hollweg, J. V.: 1991, in P. Ulmschneider, E. R. Priest and R. Rosner (eds.) 'Alfvén Waves', Mechanisms of Chromospheric and Coronal Heating, Springer-Verslag, Berlin, P.423.
Hollweg, J. V. and Yang, G.: 1988, J. Geophys. Res. 93, 5423.
Ionson, J. A.: 1978, Astrophys. J. 226, 650.
Ionson, J. A.: 1985, Solar Phys. 100, 289.
Kappraff, J. M. and Tataronis, J. A.: 1977, J. Plasma Phys. 18, 209.
Keppens, R.: 1996, Astrophys. J. 468, 907.
Lou, Y.-Q.: 1990, Astrophys. J. 350, 452.
Meerson, B. I., Sasorov, P. V. and Stepanov, A. V.: 1978, Solar Physics 58, 165.
Morse, P. M., Feshbach, H.: 1953, Methods of Theoretical Physics, McGraw-Hill Book Company, New York.
Poedts, S., Beliën, J. C. and Goedbloed, J. P.: 1994, Solar Physics 151, 271.
Poedts, S., Kerner, W. and Goossens, M.: 1989, Solar Phys. 123, 83.
Poedts, S., Goossens, M. and Kerner, W.: 1990a, Astrophys. J. 360, 279.
Poedts, S., Goossens, M. and Kerner, W.: 1990b, Computer Phys. Comm. 59, 75.
Rae, I. C. and Roberts, B.: 1983, Solar Phys. 84, 99.
Roberts, B. and Webb, A. R.: 1978, Solar Physics 56, 5.
Roberts, B. and Webb, A. R.: 1979, Solar Pysics 64, 77.
Sakurai, T., Goossens, M. and Hollweg, J. V.: 1991a, Solar Physics 133, 227.
Sakurai, T., Goossens, M. and Hollweg, J. V.: 1991b, Solar Physics 133, 247.
Spruit, H. C.: 1982, Solar Physics 75, 3.
Stenuit, H., Erdélyi, R. and Goossens, M.: 1995, Solar Phys. 161, 139.
Stenuit, H., Poedts, S. and Goossens, M.: 1993, Solar Physics 147, 13.
Tataronis,J. and Grossmann, W.: 1973, Z.Phys. 261, 203.
Wentzel, D.G.: 1979, Astron. Astrophys. 76, 20.

This article was processed by the author using Springer-Verlag LaTeX A&A style file *L-AA* version 3.